PAPER

Thickness-dependent phase transition kinetics in lithium-intercalated MoS_2

To cite this article: Joshua V Pondick *et al* 2022 *2D Mater.* **9** 025009

IOP Publishing 2D Mater. 9 (2022) 025009 https://doi.org/10.1088/2053-1583/ac4e9b

2D Materials

CrossMark

RECEIVED
24 November 2021

REVISED
30 December 2021

ACCEPTED FOR PUBLICATION
25 January 2022

PUBLISHED
4 February 2022

PAPER

Thickness-dependent phase transition kinetics in lithium-intercalated MoS_2

Joshua V Pondick[1,2], **Sajad Yazdani**[1,2], **Aakash Kumar**[1,2], **David J Hynek**[1,2], **James L Hart**[1,2], **Mengjing Wang**[1,2], **Diana Y Qiu**[1,2] and **Judy J Cha**[1,2,*]

[1] Department of Mechanical Engineering and Materials Science, Yale University, New Haven, CT 06511, United States of America
[2] Energy Sciences Institute, Yale West Campus, West Haven, CT 06516, United States of America
[*] Author to whom any correspondence should be addressed.

E-mail: judy.cha@yale.edu

Keywords: MoS_2, lithium intercalation, phase transition

Supplementary material for this article is available online

Abstract

The phase transitions of two-dimensional (2D) materials are key to the operation of many devices with applications including energy storage and low power electronics. Nanoscale confinement in the form of reduced thickness can modulate the phase transitions of 2D materials both in their thermodynamics and kinetics. Here, using *in situ* Raman spectroscopy we demonstrate that reducing the thickness of MoS_2 below five layers slows the kinetics of the phase transition from 2H- to 1T′-MoS_2 induced by the electrochemical intercalation of lithium. We observe that the growth rate of 1T′ domains is suppressed in thin MoS_2 supported by SiO_2, and attribute this growth suppression to increased interfacial effects as the thickness is reduced below 5 nm. The suppressed kinetics can be reversed by placing MoS_2 on a 2D hexagonal boron nitride (*h*BN) support, which readily facilitates the release of strain induced by the phase transition. Additionally, we show that the irreversible conversion of intercalated 1T′-MoS_2 into Li_2S and Mo is also thickness-dependent and the stability of 1T′-MoS_2 is significantly increased below five layers, requiring a much higher applied electrochemical potential to break down 1T′-MoS_2 into Li_2S and Mo nanoclusters.

1. Introduction

Two-dimensional (2D) materials exhibit a layer-dependent electronic band structure that results in tunable electronic and optoelectronic properties [1–3]. Transition metal dichalcogenides (TMDs) are of particular interest for many applications due to their numerous structural polymorphs, which yield semiconducting, semimetallic, superconducting, and topological phases [4]. Phase transitions in 2D TMDs can be controlled via doping, intercalation, and temperature [4, 5], and many of these transitions have potential applications in energy storage [6, 7], the production of chemical fuels [8, 9], non-volatile memory [10], intercalation-induced superconductivity [11–16], and neuromorphic computing [17–19]. For these applications, phase transitions in monolayer or few-layer thick TMDs are desired to reduce power consumption and for scalability. However, at this thickness limit, the thermodynamics and kinetics of phase transitions can change dramatically. Nanoscale confinement effects on phase transitions include suppressed nucleation [20, 21] and increased interfacial effects on nucleation and growth of new phases [22–25]. In particular, interfacial effects become increasingly important with thickness confinement, where interactions between 2D materials and their support substrate can induce mechanical strain [26–29], which can modulate the bandgap of 2D materials for optoelectronic applications [30–32], modify their catalytic properties [33], influence intercalation dynamics [34], and even induce phase transitions [35, 36]. Therefore, it is important to understand the effects of thickness confinement of 2D TMDs on their phase transition dynamics during intercalation. We have previously shown heterointerface effects on lithium intercalation-induced phase transitions in MoS_2 [37, 38], demonstrating one aspect of nanoscale confinement. However, confinement effects with reduced thickness have not been studied experimentally for electrochemically intercalated TMDs, while theoretical studies mostly focus on monolayer systems.

Here we investigate the effect of thickness on the structural transition in MoS_2 from the trigonal prismatic, semiconducting 2H phase to the octahedral, semimetallic 1T′ phase [39–44] induced by donated electron density [4] from lithium intercalated into the van der Waals (vdW) gaps. Using electrochemical microreactors [37, 38, 45–49], we perform electrochemical lithium intercalation into exfoliated MoS_2 flakes with thicknesses ranging from bilayers to over 20 layers, supported on SiO_2/Si or hexagonal boron nitride (*h*BN) substrates. During the intercalation induced phase transition, we used *in situ* Raman spectroscopy to observe that the growth rate of the 1T′ phase is suppressed as the thickness of MoS_2 is reduced below five layers. This kinetic suppression is attributed to mechanical strain induced during the phase transition, which has a more pronounced effect as flake thickness is reduced. Replacing the SiO_2 support substrate with 2D *h*BN reversed the observed kinetic suppression. As an *h*BN support can facilitate the rapid release of mechanical strain owing to its atomically flat surface and weak vdW interactions with MoS_2, we demonstrate that, at reduced thickness, substrate interactions can be used to control the intercalation dynamics of 2D materials.

2. Experimental details

2.1. Device fabrication

MoS_2 (SPI Supplies) and *h*BN (HQ Graphene) flakes were mechanically exfoliated from bulk crystals onto SiO_2/Si substrates using the scotch-tape method. The substrates were sonicated in acetone and isopropyl alcohol, and treated with O_2 plasma prior to exfoliation. Thin MoS_2 flakes (<10 layers) were identified via the separation between the E_{2g} and A_{1g} Raman modes (figure S1 available online at stacks.iop.org/2DM/9/025009/mmedia) measured using a Horiba LabRAM HR Evolution Spectrometer with a 532 nm laser and 1800 lines mm^{-1} diffraction grating. The thickness of MoS_2 flakes >10 layers was determined using atomic force microscopy (AFM) (figure S1) using an Asylum Research Cypher ES Environmental AFM in peak-force tapping mode. The thickness of *h*BN flakes was estimated with optical microscopy.

MoS_2 flakes of desired size and thickness were transferred to SiO_2/Si substrates using a KOH-assisted technique, as we describe previously [34, 38]. Heterostructures were fabricated by first transferring multilayer hBN flakes onto SiO_2/Si substrates using the KOH-assisted technique. All substrates for this study were commercially available Si wafers covered with a 300 nm layer of wet SiO_2 (University-Wafer, Inc.). Then MoS_2 flakes were transferred and aligned on top of the *h*BN flakes to form heterostructures. For electrochemical lithium intercalation, electrodes were patterned onto MoS_2 with electron beam lithography (Nabity NPGS, Helios G4 focused ion beam (FIB)–scanning electron microscope (SEM)) and then 10 nm Cr/100 nm Au was deposited using thermal evaporation (Mbraun EcoVap) (figure 1(a)).

2.2. Electrochemical cell fabrication

For all experiments, intercalation was conducted using an enclosed cell that holds the device and electrolyte and is sealed with an optical-grade glass top cover, as we describe previously [37, 38]. Cr/Au-contacted MoS_2 flakes and Li metal on Cu inserted into the cell serve as the working and counter/reference electrodes, respectively (figure 1(b)). For experiments with liquid electrolyte, a solution of 1 M lithium hexafluorophosphate in 50/50 v/v ethylene carbonate/diethyl carbonate (LiPF6 in EC/DEC, Sigma Aldrich), was used to fill the cell. For experiments with polymer electrolyte [50], 12 wt% of lithium bis(trifluoromethane)sulfonimide salt (Sigma Aldrich) was added to a mixture of 60 wt% poly(ethylene glycol) methyl ether methacrylate (PEGMA, Sigma Aldrich) and 25 wt% bisphenol A ethoxylate dimethacrylate (BEMA, Sigma Aldrich) and stirred for at least 4 h before adding 3 wt% of a photoinitator, 2-hydroxy-2-methyl-1-phenyl-1-propanone (Sigma Aldrich). After stirring the mixture for an additional hour, the viscous polymer electrolyte was poured into the electrochemical cell as a liquid. Once it covered the anode and cathode, illumination for 10 min with a 4 W, 375 nm UV light cured the polymer to a solid. All electrochemical cell fabrication was performed inside an argon glovebox.

2.3. Sample characterization

Intercalation cells were connected to a Biological SP300 potentiostat/galvanostat for the electrochemical intercalation of Li^+. Before intercalation, a Raman spectrum was taken at open circuit voltage (OCV, ∼2.7 V vs Li/Li^+). Lithium was intercalated into MoS_2 potentiostatically by dropping the electrochemical voltage (V_{EC}) vs Li/Li^+ at a scan rate of 10 mV s^{-1}. *In situ* Raman spectra were collected with a 633 nm laser using a Horiba LabRAM HR Evolution Spectrometer while the cell was held at a fixed V_{EC}. We note that due to the low intensity of the E_{2g} peak of *h*BN, it is not possible to monitor hBN during intercalation [37, 38].

Post intercalation, microreactors were disassembled to recover the MoS_2 devices. Recovered devices were placed into an isopropyl alcohol wash, dried, and then characterized with optical microscopy, Raman spectroscopy, and SEM (Helios G4 FIB-SEM) at tilt angles of 0° and 40°.

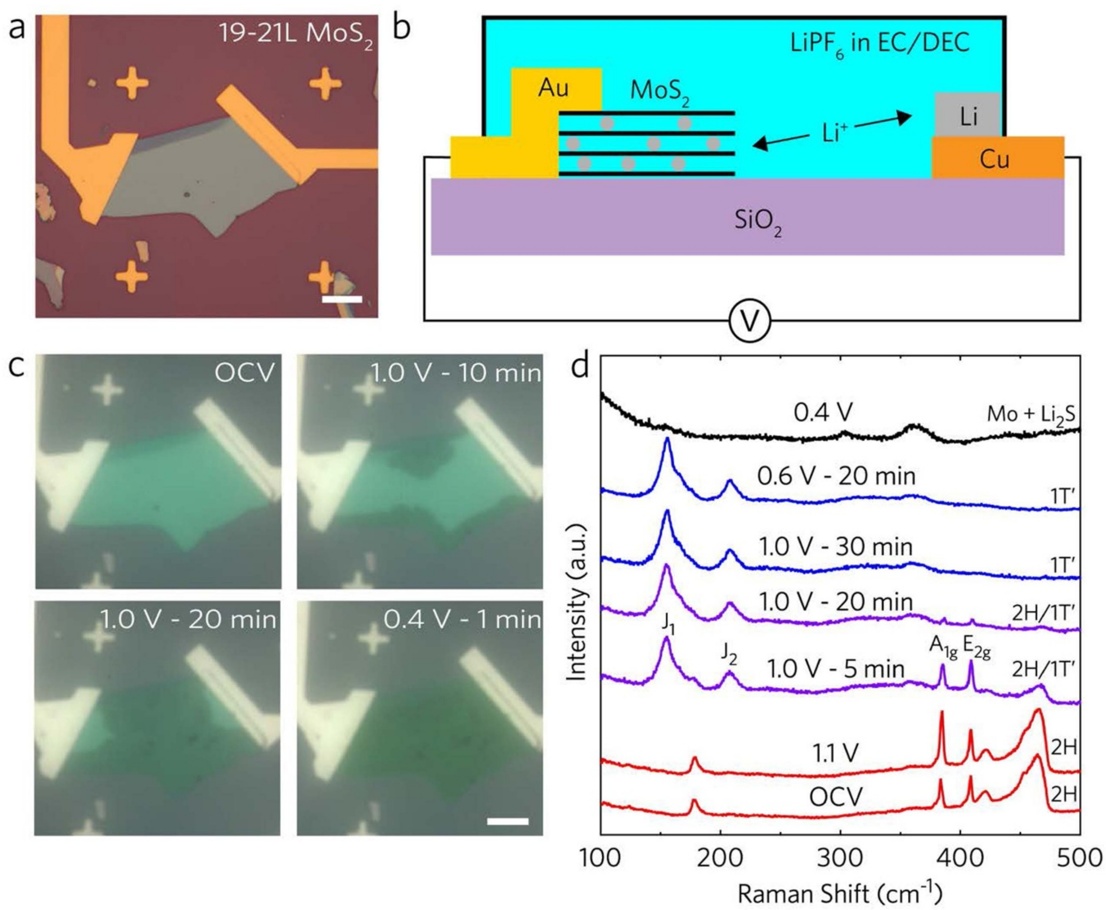

Figure 1. Li^+ intercalation of thick MoS_2. (a) Optical micrograph of a 19–21 layer MoS_2 flake with Cr/Au contacts, scale bar 10 μm. (b) Schematic cross-section of an electrochemical microreactor for intercalating lithium into MoS_2. (c) *In situ* optical micrographs of the flake in (a) at OCV, 1.0 V vs Li/Li^+ and 0.4 V vs Li/Li^+, scale bars 10 μm. The dark discoloration at 1.0 V vs Li/Li^+ indicates the presence of the 1T′ phase, while the further discoloration at 0.4 V vs Li/Li^+ to a green hue indicates the onset of the conversion reaction. (d) *In situ* Raman spectra of the device shown in (a) and (c), with red, purple, blue, and black indicating the 2H, mixed 2H/1T′, 1T′, and amorphous phases, respectively. The peaks at 303 cm^{-1} and 362 cm^{-1} are attributed to the Si substrate and electrolyte, receptively.

2.4. *Ab initio* calculations

To model the binding energy of the 2H–1T MoS_2 interface that occurs during the phase transition, density functional theory calculations within the Generalized Gradient approximation of Perdew *et al* [51] were carried out using the Projector Augmented Wave approach [52] pseudopotentials [53] as implemented in the Quantum Espresso [54] software package. The vdW interactions were included using Grimme's D3 [55] dispersion correction. In all our simulations, the more symmetric 1T structure was analyzed in place of the distorted 1T′ structure to reduce computational time, and because it is an intermediate state in the phase change sequence (2H to 1T to 1T′) of monolayer MoS_2 [56].

To model the effect of varying the thickness of 2H-MoS_2 on the 2H to 1T phase transition, we studied supercells containing a 1×1 monolayer of 1T-MoS_2 stacked on a 1×1 bilayer, four-layer, or six-layer 2H-MoS_2. In each case, 2H-MoS_2 was strained in-plane by +0.6% to match the 1T-MoS_2 equilibrium lattice parameters based on experimentally observed in-plane tensile strain in the 2H samples (<10 layers), and the whole system was allowed to relax in the direction normal to the interface. A 1040 eV cut-off for the kinetic energy of the plane waves in the basis of the wavefunctions was used and a Gamma-centered Monkhorst-Pack grid [57] of $24 \times 24 \times 1$ k-points in reciprocal space was used for all the calculations. The atoms were allowed to relax until the total energy converged to within 0.1 meV/atom and the force on each atom was less than 0.003 eV Å^{-1}. A 25 Å layer of vacuum on each of the supercells was used in our calculations. The binding energy E_{bind}, was calculated as follows,

$$E_{\mathrm{bind}} = \frac{\mathrm{E}_{2\mathrm{H}-1\mathrm{T}} - (\mathrm{E}_{2\mathrm{H}^*} + \mathrm{E}_{1\mathrm{T}})}{A}, \quad (1)$$

where $E_{2\mathrm{H}-1\mathrm{T}}$, $E_{2\mathrm{H}*}$ and $E_{1\mathrm{T}}$ are the total energies of the supercells of 2H–1T-, the 2H- (* implies strained), and 1T-MoS_2, while A is the cross-sectional area of 2H–1T heterostructure.

3. Results

We first describe the observed phase transitions of thick MoS_2 flakes, which are consistent with previous reports [45, 46, 58, 59]. Optical microscopy of a ∼20-layer MoS_2 flake during intercalation revealed that a dark discoloration grew inwards from the edge of the flake at a V_{EC} of 1.0 V vs Li/Li^+ (figures 1(c) and S2). This color change is indicative of a phase transition to the 1T′ phase [37, 38, 46], which we confirmed with *in situ* Raman spectroscopy via the suppression of the E_{2g} and A_{1g} Raman modes of 2H-MoS_2 and the simultaneous growth of the J_1 and J_2 modes of 1T′-MoS_2 (figure 1(d)) [60, 61]. After 30 min at 1.0 V vs Li/Li^+, only the J_1 and J_2 modes of the 1T′ phase were visible, indicating a complete transition to the 1T′ phase. When V_{EC} was lowered to 0.4 V vs Li/Li^+, the J_1 and J_2 peaks disappeared and an additional optical change occurred (figures 1(c) and (d)). The disappearance of all Raman peaks at 0.4 V vs Li/Li^+ indicated that MoS_2 was irreversibly converted to Mo clusters and Li_2S induced by a high concentration of intercalated lithium [45, 58]. The same intercalation dynamics were observed in MoS_2 flakes of 12–14 layers and 24–26 layers (figure S3). These results indicate that for thick MoS_2 flakes, the 2H–1T′ phase transition occurs and completes at 1.0 V vs Li/Li^+, and the conversion of MoS_2 to Mo and Li_2S occurs at 0.4 V vs Li/Li^+.

We next investigated the intercalation of thinner MoS_2 flakes. Just as in thick MoS_2, we observed the complete phase transition in a five to six layer flake at 1.0 V vs Li/Li^+ and the onset of the conversion reaction at 0.4 V vs Li/Li^+ (figure S4). In contrast to the five and six layer flake, the intercalation dynamics of a four-layer MoS_2 flake showed different behavior (figure 2(a)). A stable 2H/1T′ mixed phase, characterized by the co-presence of the Raman modes of both the 2H and 1T′ phases, was observed at 1.0 V vs Li/Li^+. This mixed 2H/1T′ phase persisted for 40 min with little change in the relative intensities of the 2H and 1T′ Raman modes. In contrast, thicker flakes showed a rapid increase in the intensity ratio of 1T′:2H Raman modes over about 10 min at 1.0 V vs Li/Li^+ (figures 1 and S2). The complete phase transition in the four-layer flake was not observed until V_{EC} was lowered to 0.8 V vs Li/Li^+, suggesting that the phase transition kinetics were markedly slower in this flake than for thick MoS_2. This stable 2H/1T′ mixed phase was also observed in the intercalation of an additional four-layer flake (figure S5). Since the 1T′ phase still nucleated at 1.0 V vs Li/Li^+, we conclude that only the kinetics of the phase transition were suppressed in four-layer MoS_2, while the thermodynamics did not change. Additionally, we observed that in all four-layer samples, the 1T′ phase persisted at 0.4 V vs Li/Li^+ instead of becoming amorphous, and a V_{EC} of 0.2 V vs Li/Li^+ was required to induce the conversion reaction to LiS_2 and Mo clusters (figures 2(a) and S5).

While four-layer MoS_2 exhibited a stable 2H/1T′ mixed phase persisting for a long time at 1.0 V vs Li/Li^+, flakes thinner than four layers showed different behavior. When three-layer MoS_2 was intercalated to 1.0 V vs Li/Li^+, the Raman peaks of the 2H phase disappeared while the J_1 peak of the 1T′ phase emerged; however, the intensity of the J_1 peak was extremely low (figure 2(b)). This weak 1T′ phase persisted for 40 min at 1.0 V vs Li/Li^+, indicating 1T′ domains did not grow over the duration of 40 min. Only when V_{EC} was lowered to 0.9 V vs Li/Li^+, did the intensity of the J_1 mode grow significantly, and the J_2 mode also emerged (figure 2(b)). This behavior suggests that while the 1T′ phase nucleated at 1.0 V, the growth of these nuclei was suppressed, and additional V_{EC} was required to induce noticeable growth of 1T′ nuclei. This suppressed growth was also observed in a four-layer flake and two additional three-layer flakes (figures S5 and S6). Additionally, just as with the four-layer flakes, the onset of the conversion reaction to Mo clusters and Li_2S occurred at 0.2 V vs Li/Li^+ in three-layer MoS_2 (figures 2(b) and S6).

Further reduction of MoS_2 thickness to two layers revealed a similar suppressed nucleation of the 1T′ phase; however, the 2H Raman modes persisted for 40 min at 1.0 V vs Li/Li^+ and did not disappear until 0.9 V vs Li/Li^+ (figure 2(c)). The bilayer MoS_2 then did not show significant growth of the 1T′ phase until V_{EC} was lowered to 0.8 V vs Li/Li^+. This suggests that for bilayer samples, the nucleation barrier to the phase transition was slightly increased in addition to the suppression of the growth kinetics of the 1T′ phase. The breakdown of MoS_2 to Mo and Li_2S was not observed at a V_{EC} of 0.2 V vs Li/Li^+ (figure 2(c)), and further intercalation to induce it was not possible due to the alloying of the gold electrodes with lithium at the low electrochemical potential [62, 63], which destroyed the contacts (figure S7).

We thus demonstrate that the kinetics of the intercalation-induced phase transition in MoS_2 are thickness-dependent. Using the *in situ* Raman data collected from MoS_2 flakes of varying thicknesses, we construct a phase diagram of intercalated MoS_2 as a function of flake thickness and V_{EC} (figure 3). We observe two features of decelerated growth of the 1T′ phase at 1.0 V vs Li/Li^+: the stable coexistence of the 2H and 1T′ phases in four-layer flakes and the presence of low-intensity 1T′ Raman peaks that only increase in intensity when V_{EC} is decreased by about 0.1 V. For thicker samples, we observe no suppression of the growth kinetics of the 1T′ phase at 1.0 V vs Li/Li^+. The same suppressed growth kinetics of the 1T′ phase was observed using a polymer electrolyte (figure S8). Furthermore, we observe that the onset of the conversion reaction from 1T′ MoS_2 to Li_2S and Mo clusters is also thickness dependent,

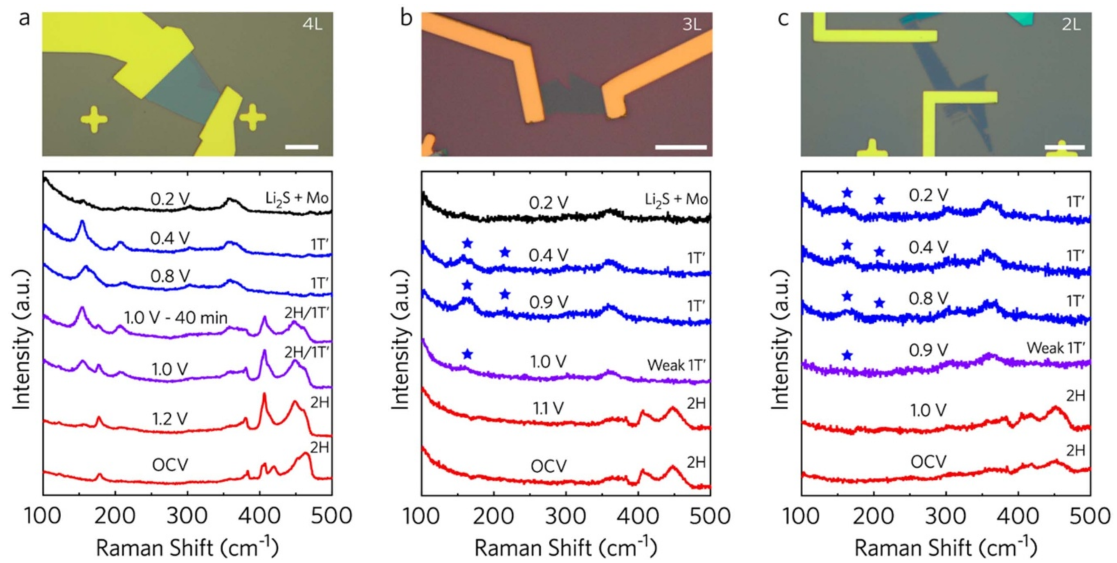

Figure 2. Li^+ intercalation of MoS_2 flakes thinner than five layers. Optical images of MoS_2 devices (top, scale bars 10 μm) and *in situ* Raman spectra (below) taken during the intercalation. The four-layer (a), three-layer (b), and two-layer (c) MoS_2 flakes all begin in the 2H phase (red). They then transition to either a stable 2H/1T′ phase ((a), purple) or 1T′ phase with weak intensity ((b) and (c), purple) before transitioning to the full 1T′ phase (blue). The location of the J_1 and J_2 peaks in the two-layer and three-layer MoS_2 spectra are indicated by blue stars. The onset of the conversion to Li_2S and Mo is indicated by the black spectra.

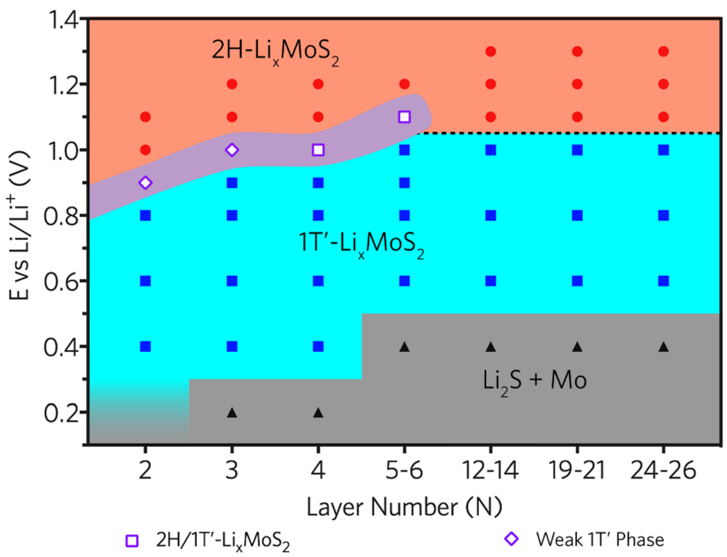

Figure 3. Phase diagram of the thickness-dependent phase transition in MoS_2. The phases of MoS_2 are plotted as a function of layer number and V_{EC}. For each thickness, the phase was measured using *in situ* Raman spectroscopy during electrochemical intercalation of lithium. The 2H phase is indicated by red shading/circles, the 1T′ phase by blue shading/squares, and the amorphous Mo + Li_2S phase by gray shading/black triangles. The dashed line indicates the potential at which the 2H–1T′ phase transition occurs in bulk MoS_2, while the purple-shaded region indicates a region of suppressed phase transition kinetics. Purple and white squares indicate the presence of a stable 2H/1T′ mixture, while purple and white diamonds indicate a very low-intensity 1T′ phase as detectable via Raman spectroscopy.

requiring an increasing applied V_{EC} as MoS_2 thickness is decreased. Our key finding is that there is a marked change in the intercalation kinetics of MoS_2 flakes thinner than five layers, as demonstrated by a slower 2H–1T′ phase transition and a delayed onset of the conversion reaction.

4. Discussion

The effect of thickness confinement on the conversion reaction to Mo and Li_2S can be understood using classical nucleation theory. An *in situ* transmission electron microscopy study previously showed formation of 2 nm Mo nanoparticles in heavily intercalated bulk MoS_2 [64], suggesting that the thermodynamically stable nucleus size for Mo clusters in a Li_2S matrix is about 2 nm. Thus, for MoS_2 thinner than four layers (corresponding to 2.5 nm in thickness), forming Mo clusters smaller than 2 nm would be thermodynamically unstable, requiring a much higher thermodynamic driving force to nucleate these metastable Mo clusters. This agrees with our observations that the V_{EC} required for the conversion reaction of MoS_2 progressively decreased from the expected 0.6 V vs Li/Li^+ for bulk flakes [45, 58] (>20 nm, figure S9), to 0.4 V vs Li/Li^+ for 5–26 layers (3–16 nm), to 0.2 V vs Li/Li^+ for three and four layers (1.9–2.5 nm), and below 0.2 V vs Li/Li^+ for bilayers (1.24 nm), as summarized in figure S10. Therefore, we conclude that as the flake thickness approaches the critical nucleus size of Mo clusters (∼2 nm) in a Li_2S matrix, the nucleation barrier for the formation of Mo clusters increases because it is necessary to nucleate Mo clusters smaller than the critical nucleus, thus requiring a higher applied V_{EC}.

To explain the suppressed growth kinetics of the 1T′ phase observed in MoS_2 flakes that are five layers and thinner, we considered several possibilities: the suppression of nucleation of the 1T′ phase with decreasing thickness, the thickness-dependent band structure of MoS_2, thickness-dependent mechanical strain, and interactions between MoS_2 and the substrate. These possibilities are discussed in order.

The first possibility is that, similar to the increased nucleation barrier for the formation of Mo clusters in Li_2S, the nucleation of the 1T′ phase could also be suppressed due to nanoscale confinement, potentially limiting the number of 1T′ nuclei and causing a slower growth of the 1T′ phase. Lateral confinement is not expected to affect the phase transition as all of the intercalated flakes have micron-scaled lateral dimensions, and previous studies have observed that the nucleation of the 1T′ phase results in the formation of nanoscaled domains in the basal planes of MoS_2 [41, 64–67]. Vertically confining the layers may suppress nucleation of the 1T′ phase if forming 2H–1T′ heterointerfaces is energetically disfavored. To investigate the possibility of vertical confinement, we used *ab initio* calculations to estimate the binding energy of the interface between bilayer, four-layer, and six-layer 2H-MoS_2 and a monolayer of 1T-MoS_2 (figure S11). We found the binding energy remains approximately constant irrespective of thickness confinement, suggesting that the nucleation of 1T′-MoS_2 should not be influenced by flake thickness. Therefore, we rule out the possibility of suppressed nucleation of the 1T′ phase to explain the observed slow kinetics in MoS_2 nanoflakes thinner than five layers.

The increase in the bandgap of MoS_2 as thickness decreases could modulate the phase transition dynamics. Computational simulations of electron doping [68] and chemical intercalation of lithium [69] suggest that decreasing the thickness of MoS_2 will lead to an increase in the critical electron concentration required to induce the 2H–1T′ phase transition. The predicted increase in critical electron concentration rapidly diminishes from monolayer to trilayer MoS_2 [68, 69], mirroring the rapid change in bandgap within this thickness regime [70]. As flake thickness approaches five layers, the increase in critical electron concentration needed for the phase transition is negligible. For all MoS_2 flakes three layers and thicker, we observed the nucleation of the 1T′ phase at 1.0 V vs Li/Li^+, in agreement with the calculations. We did observe a small increase of 0.1 V in the V_{EC} required to induce the phase transition in bilayer MoS_2 (figure 2(c)). Therefore, we can attribute the slight increase in the V_{EC} required to nucleate the 1T′ phase in bilayer MoS_2 to bandgap-modulated thermodynamics. Once the 1T′ phase is nucleated in the bilayer sample, we observe similar delayed kinetics as in the other thicknesses of MoS_2, indicating that the thermodynamic and kinetic effects on the phase transition are separate phenomena.

While the increased bandgap can explain the observed phase transitions in bilayer MoS_2, it does not explain the suppressed growth of the 1T′ phase for three to four layer MoS_2. The third possibility is intercalation induced mechanical strain that could modulate the phase transition dynamics of MoS_2. As lithium is intercalated into MoS_2, the interlayer spacing expands [59, 71]; however, the gold top contacts in our devices act as mechanical clamps to prevent this expansion for the regions of MoS_2 directly underneath the gold, causing the flake to bend. We previously demonstrated [34] that in-plane strain induced by this bending can delay the formation of lithium ordering in graphene microflakes. Similar bending-induced strain may decelerate the phase transition kinetics in MoS_2 during intercalation. To probe this, we analyzed the peak position of the E_{2g} mode of 2H-MoS_2 during intercalation (figure S12) as the E_{2g} mode is highly sensitive to in-plane strain [72, 73], while unchanged by electron doping [74, 75]. As V_{EC} was lowered from OCV for all flakes five to six layers and thinner, the E_{2g} peak red-shifted, indicating tensile strain [31, 32, 76–78]. In contrast, the E_{2g} peak of flakes thicker than ten layers showed a blue-shift characteristic of compressive strain [79, 80]. Computational studies have predicted that in-plane tensile strain should facilitate the phase transition of MoS_2 by reducing the energy gap between the 2H and 1T′ phases [36, 81]. Despite this prediction, we observed the opposite trend: thinner flakes under tensile strain had slower phase transition kinetics than thicker flakes under compressive strain. Therefore, we conclude that the slower phase transition observed in thin MoS_2 occurred in spite of rather than due to lithium-induced mechanical strain.

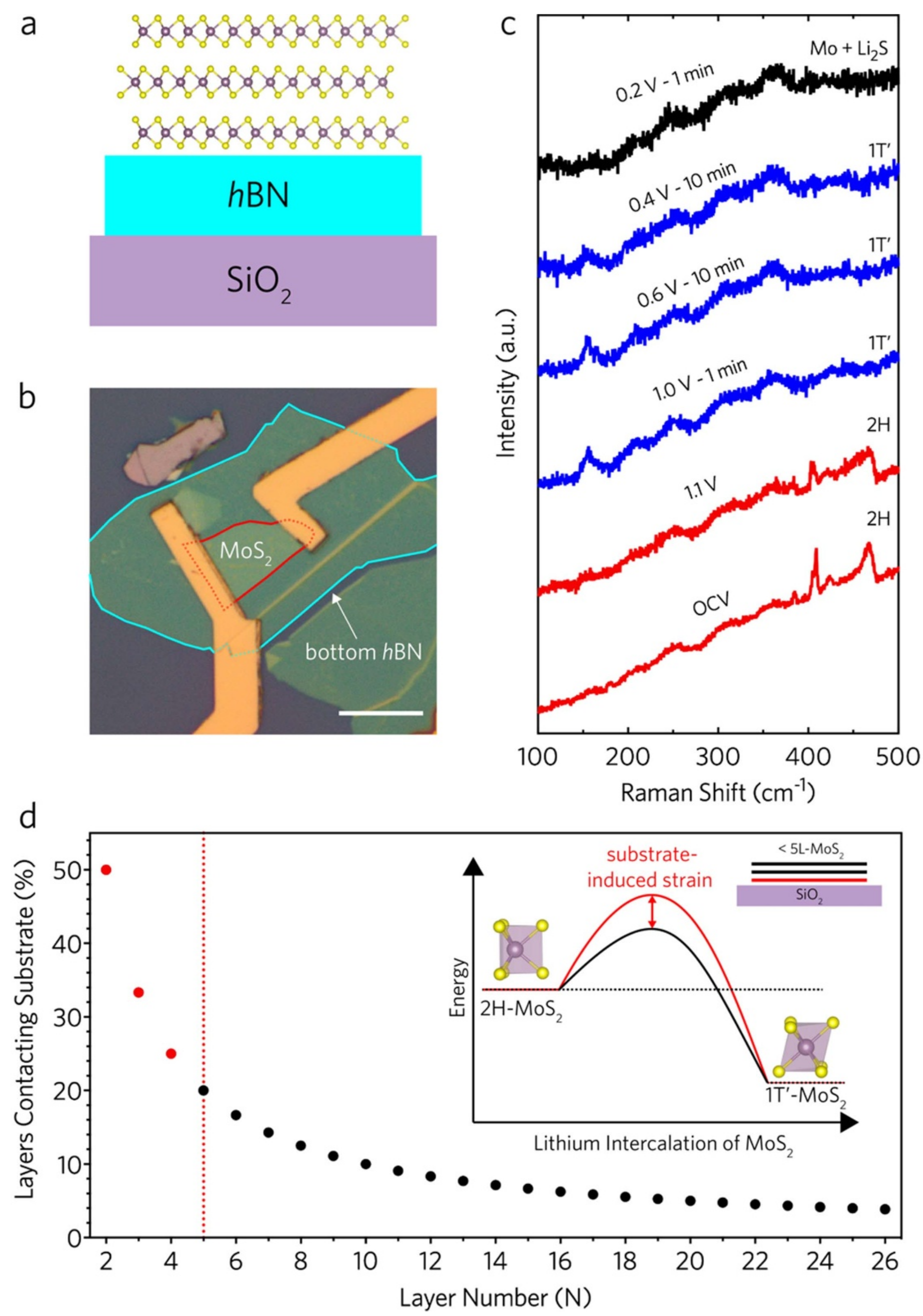

Figure 4. Substrate effects on phase transition kinetics. (a) Schematic cross-section of a heterostructure between trilayer MoS_2 (atomic structure; Mo and S atoms are colored purple and yellow, respectively) and multilayer *h*BN (cyan). Thickness is not shown to scale. (b) Optical micrograph of a trilayer MoS_2 flake (red) placed on top of multilayer *h*BN (cyan) with gold contacts to MoS_2; scale bar, 10 μm. (c) *In situ* Raman spectra taken of the device in (b) during lithium intercalation. MoS_2 remained in the 2H phase (red) until 1.0 V vs Li/Li^+, when it transitioned to the 1T′ phase (blue). (d) Fraction of MoS_2 layers directly in contact with the substrate plotted as a function of layer number. The fraction is calculated as (100%/N) since only the bottom layer is in contact with the substrate. Below five layers (dashed red line), the flakes exhibited suppressed phase transition kinetics (red dots). Inset, schematic of the proposed mechanism for the suppressed kinetics in thin flakes. The substrate-induced strain (red) dominates in thin samples, causing a slower phase transition.

Finally, we consider the influence of the substrate on the phase transition in MoS_2. Since the phase transition requires the rearrangement of the sulfur atoms, it causes in-plane mechanical strain, distinct from bending-induced strain due to expansion of vdW gaps discussed previously. The in-plane strain due to the phase transition has been observed to cause the formation of wrinkled microstructures in several-layer MoS_2 supported on SiO_2/Si substrates [46]. We previously demonstrated [37] that placing MoS_2 onto a 2D substrate such as graphene or *h*BN facilitates the formation of these wrinkled microstructures, suggesting that a 2D support may effectively release the phase-transition induced in-plane strain in MoS_2. To investigate this effect in thin MoS_2, we placed trilayer MoS_2 onto a multilayer hBN support substrate (figures 4(a) and (b)), and then contacted MoS_2 with gold. *In situ* Raman spectroscopy during intercalation revealed that unlike in the SiO_2-supported case, we did not observe a stable 2H/1T′ mixed phase or a weak 1T′ phase, but rather, the flake underwent the phase transition and showed intense J_1 and J_2 peaks immediately when V_{EC} was lowered to 1.0 V vs Li/Li^+ (figure 4(c)).

This suggests that for thin flakes, the SiO_2 substrate prevents the release of phase transition-induced mechanical strain, causing a suppression in the kinetics of the phase transition. By replacing the SiO_2 with *h*BN, the weak vdW interactions between MoS_2 and *h*BN can facilitate the rapid release of this strain, which we demonstrated in a replicate heterostructure of trilayer MoS_2 partially supported on hBN and partially supported by SiO_2 (figure S13). During intercalation, the phase transition occurred more rapidly on the *h*BN-supported region of MoS_2, and post mortem analysis revealed that this region developed a wrinkled microstructure of increased intensity and density as compared to the SiO_2-supported region. Since the fraction of MoS_2 layers that interact with the substrate increases rapidly with decreasing layer number (figure 4(d)), this effect is expected to be pronounced in flakes thinner than five layers. We note that the conversion reaction to Mo and LiS_2 occurred at 0.2 V vs Li/Li^+ for *h*BN-supported trilayer MoS_2 (figure 4(c)), indicating that *h*BN has an effect on the 2H–1T′ phase transition kinetics, but not on the delayed nucleation of Mo nanoclusters due to thickness-confinement of MoS_2.

5. Conclusions

In summary, we observed for the first time that the 2H–1T′ phase transition and subsequent conversion to Li_2S and Mo induced by the electrochemical intercalation of lithium can be modulated by the thickness of MoS_2. As the layer number is decreased to below five, interactions with the substrate suppress the ability of the flakes to release mechanical strain induced by the phase transition, slowing the growth of the 1T′ phase. The suppression of the phase transition kinetics can be alleviated by placing MoS_2 on a 2D substrate that can facilitate the release of mechanical strain. As MoS_2 is further reduced in thickness to bilayer, a slight increase in the applied V_{EC} required to nucleate the 1T′ phase is observed and attributed to an increased critical electron concentration caused by the increase in the bandgap of MoS_2. Furthermore, nanoscale confinement as flake thickness is reduced towards 2 nm likely increased the nucleation barrier to the formation of Mo nanoclusters, requiring an increased applied V_{EC} to induce the conversion reaction in thin MoS_2. As thickness-dependent properties are a prominent feature in all 2D materials, the dependence of intercalation dynamics on layer number is likely not unique to MoS_2. This has implications for many device applications that rely on phase-changes in 2D materials, suggesting that the thickness of the active layer could alter phase change dynamics and phase stability.

Data availability statement

All data that support the findings of this study are included within the article (and any supplementary files).

Acknowledgments

J V P was supported by the National Defense Science and Engineering Graduate (NDSEG) Fellowship Program, sponsored by the Air Force Research Laboratory (AFRL), the Office of Naval Research (ONR), and the Army Research Office (ARO). J J C acknowledges support from the National Science Foundation (CAREER #1749742). Device fabrication and characterization was carried out at the Yale West Campus Materials Characterization Core, the Yale West Campus Cleanroom, and the Yale West Campus Imaging Core. Theoretical and computation work by D Y Q and A K was supported by the US Department of Energy, Office of Science, Office of Basic Energy Sciences Early Career Research Program under Award Number DE-SC0021965. The calculations used resources of the National Energy Research Scientific Computing Center (NERSC), a DOE Office of Science of the US Department of Energy under Contract No. DE-AC02-05CH11231, and the Extreme Science and Engineering Discovery Environment (XSEDE), which is supported by National Science Foundation Grant Number ACI-1548562.

Conflict of interest

These authors respectfully declare that, there are no conflicts of interest to acknowledge for this research.

ORCID iDs

Joshua V Pondick https://orcid.org/0000-0003-3380-2686
Aakash Kumar https://orcid.org/0000-0003-1338-2530
David J Hynek https://orcid.org/0000-0002-8778-5319
James L Hart https://orcid.org/0000-0002-2960-6925
Mengjing Wang https://orcid.org/0000-0003-1195-4515
Diana Y Qiu https://orcid.org/0000-0003-3067-6987
Judy J Cha https://orcid.org/0000-0002-6346-2814

References

[1] Wang Q H, Kalantar-Zadeh K, Kis A, Coleman J N and Strano M S 2012 Electronics and optoelectronics of two-dimensional transition metal dichalcogenides *Nat. Nanotechnol.* **7** 699–712

[2] Li X L, Han W P, Bin W J, Qiao X F, Zhang J and Tan P H 2017 Layer-number dependent optical properties of 2D materials and their application for thickness determination *Adv. Funct. Mater.* **27** 1604468

[3] Wang C *et al* 2018 Monolayer atomic crystal molecular superlattices *Nature* **555** 231–6

[4] Chhowalla M, Shin H S, Eda G, Li L J, Loh K P and Zhang H 2013 The chemistry of two-dimensional layered transition metal dichalcogenide nanosheets *Nat. Chem.* **5** 263–75

[5] Yang H, Kim S W, Chhowalla M and Lee Y H 2017 Structural and quantum-state phase transition in van der Waals layered materials *Nat. Phys.* **13** 931–7

[6] Acerce M, Voiry D and Chhowalla M 2015 Metallic 1T phase MoS_2 nanosheets as supercapacitor electrode materials *Nat. Nanotechnol.* **10** 313–8

[7] Leng K, Chen Z, Zhao X, Tang W, Tian B, Nai C T, Zhou W and Loh K P 2016 Phase restructuring in transition metal dichalcogenides for highly stable energy storage *ACS Nano* **10** 9208–15

[8] Voiry D *et al* 2016 The role of electronic coupling between substrate and 2D MoS_2 nanosheets in electrocatalytic production of hydrogen *Nat. Mater.* **15** 1003–9

[9] Wang H *et al* 2013 Electrochemical tuning of vertically aligned MoS_2 nanofilms and its application in improving hydrogen evolution reaction *Proc. Natl Acad. Sci.* **110** 19701–6

[10] Rehn D A, Li Y, Pop E and Reed E J 2018 Theoretical potential for low energy consumption phase change memory utilizing electrostatically-induced structural phase transitions in 2D materials *npj Comput. Mater.* **4** 2

[11] Huang G Q, Xing Z W and Xing D Y 2016 Dynamical stability and superconductivity of Li-intercalated bilayer MoS_2: a first-principles prediction *Phys. Rev.* B **93** 104511

[12] Zhang J J, Gao B and Dong S 2016 Strain-enhanced superconductivity of MoX_2($X = S$ or Se) bilayers with Na intercalation *Phys. Rev.* B **93** 155430

[13] Szczęśniak R, Durajski A P and Jarosik M W 2017 Metallization and superconductivity in Ca-intercalated bilayer MoS_2 *J. Phys. Chem. Solids* **111** 254–7

[14] Szczęśniak R, Durajski A P and Jarosik M W 2018 *Ab-initio* study of superconducting state in intercalated $MoSe_2$ and WSe_2 bilayers *Physica* B **536** 773–6

[15] Szczęśniak R, Durajski A P and Jarosik M W 2018 Strong-coupling superconductivity induced by calcium intercalation in bilayer transition-metal dichalcogenides *Front. Phys.* **13** 137401

[16] Yu Y *et al* 2015 Gate-tunable phase transitions in thin flakes of 1T-TaS_2 *Nat. Nanotechnol.* **10** 270–6

[17] Yoshida M, Suzuki R, Zhang Y, Nakano M and Iwasa Y 2015 Memristive phase switching in two-dimensional 1T-TaS_2 crystals *Sci. Adv.* **1** e1500606

[18] Zhang F, Zhang H, Krylyuk S, Milligan C A, Zhu Y, Zemlyanov D Y, Bendersky L A, Burton B P, Davydov A V and Appenzeller J 2019 Electric-field induced structural transition in vertical $MoTe_2$- and $Mo_{1-x}W_xTe_2$-based resistive memories *Nat. Mater.* **18** 55–61

[19] Zhu X, Li D, Liang X and Lu W D 2019 Ionic modulation and ionic coupling effects in MoS_2 devices for neuromorphic computing *Nat. Mater.* **18** 141–8

[20] Sohn S, Jung Y, Xie Y, Osuji C, Schroers J and Cha J J 2015 Nanoscale size effects in crystallization of metallic glass nanorods *Nat. Commun.* **6** 8157

[21] Han H J, Lee G R, Xie Y, Jang H, Hynek D J, Cho E N, Kim Y J, Jung Y S and Cha J J 2021 Unconventional grain growth suppression in oxygen-rich metal oxide nanoribbons *Sci. Adv.* **7** eabh2012

[22] Zhu C, Ma J, Ge X, Rao F, Ding K, Lv S, Wu L and Song Z 2016 Low-energy phase change memory with graphene confined layer *Appl. Phys. Lett.* **108** 3–5

[23] Mio A M, Privitera S M S, Bragaglia V, Arciprete F, Cecchi S, Litrico G, Persch C, Calarco R and Rimini E 2017 Role of interfaces on the stability and electrical properties of $Ge_2Sb_2Te_5$ crystalline structures *Sci. Rep.* **7** 2616

[24] Neumann C M, Okabe K L, Yalon E, Grady R W, Wong H S P and Pop E 2019 Engineering thermal and electrical interface properties of phase change memory with monolayer MoS_2 *Appl. Phys. Lett.* **114** 82103

[25] Aryana K *et al* 2021 Interface controlled thermal resistances of ultra-thin chalcogenide-based phase change memory devices *Nat. Commun.* **12** 774

[26] Chaste J *et al* 2018 Intrinsic properties of suspended MoS_2 on SiO_2/Si pillar arrays for nanomechanics and optics *ACS Nano* **12** 3235–42

[27] Sun Y and Liu K 2019 Strain engineering in functional 2D materials *J. Appl. Phys.* **125** 082402

[28] Dai Z, Liu L and Zhang Z 2019 Strain engineering of 2D materials: issues and opportunities at the interface *Adv. Mater.* **31** 1805417

[29] Li Z *et al* 2020 Efficient strain modulation of 2D materials via polymer encapsulation *Nat. Commun.* **11** 1151

[30] Feng J, Qian X, Huang C W and Li J 2012 Strain-engineered artificial atom as a broad-spectrum solar energy funnel *Nat. Photon.* **6** 866–72

[31] Conley H J, Wang B, Ziegler J I, Haglund R F, Pantelides S T and Bolotin K I 2013 Bandgap engineering of strained monolayer and bilayer MoS_2 *Nano Lett.* **13** 3626–30

[32] Castellanos-Gomez A, Roldán R, Cappelluti E, Buscema M, Guinea F, van der Zant H S J and Steele G A 2013 Local strain engineering in atomically thin MoS_2 *Nano Lett.* **13** 5361–6

[33] Li H *et al* 2016 Activating and optimizing MoS_2 basal planes for hydrogen evolution through the formation of strained sulphur vacancies *Nat. Mater.* **15** 48–53

[34] Pondick J V, Yazdani S, Yarali M, Reed S N, Hynek D J and Cha J J 2021 The effect of mechanical strain on lithium staging in graphene *Adv. Electron. Mater.* **7** 2000981

[35] Song S, Keum D H, Cho S, Perello D, Kim Y and Lee Y H 2016 Room temperature semiconductor-metal transition of $MoTe_2$ thin films engineered by strain *Nano Lett.* **16** 188–93

[36] Duerloo K A N, Li Y and Reed E J 2014 Structural phase transitions in two-dimensional Mo- and W-dichalcogenide monolayers *Nat. Commun.* **5** 4214

[37] Pondick J V, Kumar A, Wang M, Yazdani S, Woods J M, Qiu D Y and Cha J J 2021 Heterointerface control over lithium-induced phase transitions in MoS_2 nanosheets: implications for nanoscaled energy materials *ACS Appl. Nano Mater.* **4** 14105–14

[38] Yazdani S, Pondick J V, Kumar A, Yarali M, Woods J M, Hynek D J, Qiu D Y and Cha J J 2021 Heterointerface effects on lithium-induced phase transitions in intercalated MoS_2 *ACS Appl. Mater. Interfaces* **13** 10603–11

[39] Kertesz M and Hoffmann R 1984 Octahedral vs trigonal-prismatic coordination and clustering in transition-metal dichalcogenides *J. Am. Chem. Soc.* **106** 3453–60

[40] Dungey K E, Curtis M D and Penner-Hahn J E 1998 Structural characterization and thermal stability of MoS_2 intercalation compounds *Chem. Mater.* **10** 2152–61

[41] Wang L, Xu Z, Wang W and Bai X 2014 Atomic mechanism of dynamic electrochemical lithiation processes of MoS_2 nanosheets *J. Am. Chem. Soc.* **136** 6693–7

[42] Dresselhaus M S (ed) 1986 *Intercalation in Layered Materials* (New York: Springer Science + Buisness Media LLC)

[43] Eda G, Yamaguchi H, Voiry D, Fujita T, Chen M and Chhowalla M 2011 Photoluminescence from chemically exfoliated MoS_2 *Nano Lett.* **11** 5111–6

[44] Wan J, Lacey S D, Dai J, Bao W, Fuhrer M S and Hu L 2016 Tuning two-dimensional nanomaterials by intercalation: materials, properties and applications *Chem. Soc. Rev.* **45** 6742–65

[45] Wan J *et al* 2015 *In situ* investigations of Li-MoS_2 with planar batteries *Adv. Energy Mater.* **5** 1401742

[46] Xiong F, Wang H, Liu X, Sun J, Brongersma M, Pop E and Cui Y 2015 Li intercalation in MoS_2: *in situ* observation of its dynamics and tuning optical and electrical properties *Nano Lett.* **15** 6777–84

[47] Kühne M, Paolucci F, Popovic J, Ostrovsky P M, Maier J and Smet J H 2017 Ultrafast lithium diffusion in bilayer graphene *Nat. Nanotechnol.* **12** 895–900

[48] Bediako D K, Rezaee M, Yoo H, Larson D T, Zhao S Y F, Taniguchi T, Watanabe K, Brower-Thomas T L, Kaxiras E and Kim P 2018 Heterointerface effects in the electrointercalation of van der Waals heterostructures *Nature* **558** 425–9

[49] Zhang J *et al* 2018 Reversible and selective ion intercalation through the top surface of few-layer MoS_2 *Nat. Commun.* **9** 5289

[50] Nair J R, Gerbaldi C, Destro M, Bongiovanni R and Penazzi N 2011 Methacrylic-based solid polymer electrolyte membranes for lithium-based batteries by a rapid UV-curing process *React. Funct. Polym.* **71** 409–16

[51] Perdew J P, Burke K and Ernzerhof M 1996 Generalized gradient approximation made simple *Phys. Rev. Lett.* **78** 1396

[52] Blöch P E 1994 Projector augmented-wave method *Phys. Rev.* B **50** 17953–79

[53] Dal Corso A 2014 Pseudopotentials periodic table: from H to Pu *Comput. Mater. Sci.* **95** 337–50

[54] Giannozzi P *et al* 2009 QUANTUM ESPRESSO: a modular and open-source software project for quantum simulations of materials *J. Phys.: Condens. Matter* **21** 395502

[55] Grimme S, Antony J, Ehrlich S and Krieg H 2010 A consistent and accurate *ab initio* parametrization of density functional dispersion correction (DFT-D) for the 94 elements H-Pu *J. Chem. Phys.* **132** 154104

[56] Lin Y C, Dumcenco D O, Huang Y S and Suenaga K 2014 Atomic mechanism of the semiconducting-to-metallic phase transition in single-layered MoS_2 *Nat. Nanotechnol.* **9** 391–6

[57] Monkhorst H J and Pack J D 1976 Special points for Brillonin-zone integrations *Phys. Rev.* B **13** 5188–92

[58] Xiao J, Choi D, Cosimbescu L, Koech P, Liu J and Lemmon J P 2010 Exfoliated MoS_2 nanocomposite as an anode material for lithium ion batteries *Chem. Mater.* **22** 4522–4

[59] Zhang L, Sun D, Kang J, Feng J, Bechtel H A, Wang L W, Cairns E J and Guo J 2018 Electrochemical reaction mechanism of the MoS_2 electrode in a lithium-ion cell revealed by *in situ* and operando x-ray absorption spectroscopy *Nano Lett.* **18** 1466–75

[60] Jiménez Sandoval S, Yang D, Frindt R F and Irwin J C 1991 Raman study and lattice dynamics of single molecular layers of MoS_2 *Phys. Rev.* B **44** 3955–62

[61] Kappera R, Voiry D, Yalcin S E, Brittany Branch B, Gupta G, Mohite A D and Chhowalla M 2014 Phase-engineered low-resistance contacts for ultrathin MoS_2 transistors *Nat. Mater.* **13** 1128–34

[62] Taillades G, Benjelloun N, Sarradin J and Ribes M 2002 Metal-based very thin film anodes for lithium ion microbatteries *Solid State Ion.* **152–153** 119–24

[63] Zeng Z, Liang W I, Chu Y H and Zheng H 2014 *In situ* TEM study of the Li–Au reaction in an electrochemical liquid cell *Faraday Discuss.* **176** 95–107

[64] Su Q, Wang S, Feng M, Du G and Xu B 2017 Direct studies on the lithium-storage mechanism of molybdenum disulfide *Sci. Rep.* **7** 7275

[65] Ghosh C, Singh M K, Parida S, Janish M T, Dobley A, Dongare A M and Carter C B 2021 Phase evolution and structural modulation during *in situ* lithiation of MoS_2, WS_2 and graphite in TEM *Sci. Rep.* **11** 9014

[66] Petkov V, Billinge S J L, Larson P, Mahanti S D, Vogt T, Rangan K K and Kanatzidis M G 2002 Structure of nanocrystalline materials using atomic pair distribution function analysis: study of $LiMoS_2$ *Phys. Rev.* B **65** 092105

[67] Quilty C D *et al* 2019 Ex situ and operando XRD and XAS analysis of MoS_2: a lithiation study of bulk and nanosheet materials *ACS Appl. Energy Mater.* **2** 7635–46

[68] Sun X, Wang Z, Li Z and Fu Y Q 2016 Origin of structural transformation in mono- and bi-layered molybdenum disulfide *Sci. Rep.* **6** 26666

[69] Sun L *et al* 2018 Layer-dependent chemically induced phase transition of two-dimensional MoS_2 *Nano Lett.* **18** 3435–40

[70] Mak K F, Lee C, Hone J, Shan J and Heinz T F 2010 Atomically thin MoS_2: a new direct-gap semiconductor *Phys. Rev. Lett.* **105** 136805

[71] Sharma N, Du G, Studer A J, Guo Z and Peterson V K 2011 *In-situ* neutron diffraction study of the MoS_2 anode using a custom-built Li-ion battery *Solid State Ion.* **199–200** 37–43

[72] Lee C, Yan H, Brus L, Heinz T, Hone J and Ryu S 2010 Anomalous lattice vibrations of single- and few-layer MoS_2 *ACS Nano* **4** 2695–700

[73] Li S L, Miyazaki H, Song H, Kuramochi H, Nakaharai S and Tsukagoshi K 2012 Quantitative Raman spectrum and reliable thickness identification for atomic layers on insulating substrates *ACS Nano* **6** 7381–8

[74] Kukucska G and Koltai J 2017 Theoretical investigation of strain and doping on the Raman spectra of monolayer MoS_2 *Phys. Status Solidi* b **254** 1700184

[75] Zou J, Li F, Bissett M A, Kim F and Hardwick L J 2020 Intercalation behavior of Li and Na into three-layer and multilayer MoS_2 flakes *Electrochim. Acta* **331** 135284

[76] Wang Y, Cong C, Qiu C and Yu T 2013 Raman spectroscopy study of lattice vibration and crystallographic orientation of monolayer MoS_2 under uniaxial strain *Small* **9** 2857–61

[77] Lloyd D, Liu X, Christopher J W, Cantley L, Wadehra A, Kim B L, Goldberg B B, Swan A K and Bunch J S 2016 Band gap engineering with ultralarge biaxial strains in suspended monolayer MoS_2 *Nano Lett.* **16** 5836–41

[78] Guo Y *et al* 2020 Direct bandgap engineering with local biaxial strain in few-layer MoS_2 bubbles *Nano Res.* **13** 2072–8

[79] Alencar R S, Saboia K D A, Machon D, Montagnac G, Meunier V, Ferreira O P, San-Miguel A and Souza Filho A G 2017 Atomic-layered MoS_2 on SiO_2 under high pressure: bimodal adhesion and biaxial strain effects *Phys. Rev. Mater.* **1** 024002

[80] Nayak A P, Bhattacharyya S, Zhu J, Liu J, Wu X, Pandey T, Jin C, Singh A K, Akinwande D and Lin J F 2014 Pressure-induced semiconducting to metallic transition in multilayered molybdenum disulphide *Nat. Commun.* **5** 3731

[81] Tang Q 2018 Tuning the phase stability of Mo-based TMD monolayers through coupled vacancy defects and lattice strain *J. Mater. Chem.* C **6** 9561–8